

Article

Research on Radiation Damage and Reinforcement of Control and Sensing Systems in Nuclear Robots

Yinlin Chang ^{1,2}, Shuliang Zou ^{1,2} , Guang Lin ¹, Dewen Tang ^{2,3}, Cuiyue Wei ^{1,2} and Shoulong Xu ^{1,2,*} 

¹ School of Resource Environment and Safety Engineering, University of South China, 28, West Changsheng Road, Hengyang 421001, China; 20231002110011@stu.usc.edu.cn (Y.C.); wcy@stu.usc.edu.cn (C.W.)

² Provincial Key Laboratory of Emergency Safety Technology and Equipment for Nuclear Facilities, University of South China, Hengyang 421001, China

³ School of Mechanical Engineering, University of South China, Hengyang 421001, China

* Correspondence: xusl@usc.edu.cn; Tel.: +86-152-1181-2766

Abstract: This study investigates the radiation damage and radiation reinforcement of the control and sensing systems of nuclear robots. Radiation experiments were conducted on key electronic devices to study their radiation resistance, and a shielding structure for radiation reinforcement was designed to meet the radiation resistance performance requirements of the system. The results show that at doses exceeding 1300 Gy, Hall sensors, pressure transducers, and temperature transducers exhibit radiation damage. At doses exceeding 170 Gy, transformers and controllers also show radiation damage. Lithium batteries remain largely unaffected, but packs experience voltage decline. When using Pb and W as shielding materials for Super MC simulation, it was found that at a thickness of 15 mm, the shielding efficiency of the controller and transformer under Pb shielding increased by approximately 84.99% and 52.00%, respectively, compared to 92.23% and 74.47% under W, which had the best shielding effect benefits. By adopting radiation-resistant shielding reinforcement, we can effectively improve the radiation resistance of the controller and transformer. This is crucial for ensuring the reliable operation of nuclear robots in high-radiation environments and providing important data and theoretical support for the development of related technologies.

Keywords: robot; radiation; reinforcement; γ -ray; superMC; control and sensing systems



Citation: Chang, Y.; Zou, S.; Lin, G.; Tang, D.; Wei, C.; Xu, S. Research on Radiation Damage and Reinforcement of Control and Sensing Systems in Nuclear Robots. *Electronics* **2024**, *13*, 1214. <https://doi.org/10.3390/electronics13071214>

Academic Editors: Dah-Jye Lee and Luca Patané

Received: 13 February 2024

Revised: 19 March 2024

Accepted: 22 March 2024

Published: 26 March 2024



Copyright: © 2024 by the authors. Licensee MDPI, Basel, Switzerland. This article is an open access article distributed under the terms and conditions of the Creative Commons Attribution (CC BY) license (<https://creativecommons.org/licenses/by/4.0/>).

1. Introduction

Nuclear robot technology plays a crucial role in nuclear emergencies, allowing operators to take swift and accurate measures while avoiding radiation exposure. Traditional robots face reliability issues in high-radiation areas when their control and sensing systems are damaged, highlighting the importance of enhancing the reliability of robotic nuclear emergency operations to ensure stable and safe remote work in high-radiation environments. The application of nuclear robots has become a key solution to this challenge, as they can perform complex tasks, reduce personnel exposure risks, and enhance the efficiency of emergency responses [1,2]. Han Yi, Wang Chuan, and Chi Xiaomiao [3] obtained the failure dose threshold of various electronic devices through screening and failure-rate analysis of robot electronic devices. Then, through partition design, sensitive components with low threshold values are grouped together for unified management and replacement, achieving radiation shielding reinforcement design. Liu Zhenzhong [4] analyzed the radiation damage mechanism of power system components, identifying significant radiation impacts on solar cells and power MOS devices. Chen Faguo and Zhu Wanning [5] introduced the radiation-resistant design and testing of remote-controlled robots working in strong radiation environments. Based on the damage to robot electronic devices, the local shielding designs of control circuits and core circuits were implemented. The experimental result demonstrated that the robot could operate normally in a strong radiation field of at least 100 Gy/h, with an initial estimate of its capacity to withstand a

cumulative dose of up to 3000 Gy. Su Kangjia and Yang Fangyan [6] studied the design and radiation protection of joint modules for special robots. They adopted active and passive methods for radiation shielding reinforcement of joint modules. The irradiation-reinforced joint modules can withstand a radiation dose of 600 Gy and operate normally. Studies on the performance changes in lithium batteries under radiation conditions show that γ -ray can lead to a reduction in the capacitance and storage capacity of lithium-ion batteries due to interactions between the internal electrolyte and the electrode [7]. High-energy electron radiation not only causes ionization damage to the oxide layer interface in electronic devices but also has a significant impact on the radiation effect of devices due to displacement damage [8–15]. He Zhaohui, Chen Wei, and Han Jianwei [16], based on the synergistic effect of the total dose response of multiple chips, researched methods to mitigate the coupling effect of total dose effects across various types of chips. Simultaneously, they explored the application of different polymers to enhance their total dose effects, guided by the degradation mechanism of polymer materials under total dose radiation. Xie Rubin, Ge Chaoyang, and Zhou Xin [17], based on the 0.18 μm BCD process, developed an NLDMOS device with radiation tolerance and improved the radiation tolerance of the device through process reinforcement measures. Although using different polymers to improve its total dose effects, process reinforcement measures, and employing partition redundancy design have increased radiation resistance capability, the high development costs, prolonged time, and increased resource and power consumption remain significant drawbacks. Despite the aforementioned literature focusing on the radiation damage of individual electronic devices, power systems, and certain functional modules, there is still no consideration for enhancing the overall radiation resistance of electronic devices and the threshold for failure of batteries and MOS devices in power systems. In addition, the development of radiation-hardened chips for nuclear robots incurs high costs and lacks guaranteed reliability, while radiation shielding structures can improve their reliability and optimize their own weight distribution. Currently, there is still no comprehensive system for evaluating the changes in performance under radiation conditions in the research on radiation damage to key components in control systems and sensing systems of nuclear robots, both domestically and internationally. There exists a deficiency in systematic research on radiation effects, radiation damage, and radiation hardening.

This article conducts research on the radiation damage and radiation shielding reinforcement of nuclear robots, building on the study of damage mechanisms and principles of various components in control and sensing systems. Through radiation experiments on radiation-sensitive control and sensing system components, we analyzed the radiation resistance lifespan of different components and their operational capabilities in radiation environments. A method for radiation shielding reinforcement targeting radiation-sensitive and vulnerable components is proposed. The findings of this study are essential for bridging the research gap in the field of nuclear robotics and laying solid theoretical and practical groundwork for future studies and applications in related domains. Nuclear robots are capable of undertaking various tasks, including radiation measurement, the maintenance of nuclear facilities, and the disposal of nuclear waste, thus mitigating human exposure to high-radiation environments. However, it is crucial to acknowledge the limitations of this study. Radiation environments may entail multiple radiation sources and intricate scenarios, yet current research tends to focus on the impact of single radiation sources. Future investigations should delve into the comprehensive effects of mixed radiation scenarios on robots and equipment to better replicate real-world working conditions. Additionally, there is a need to develop more sophisticated radiation-sensitive devices and shielding materials while enhancing the control algorithms and intelligent systems of nuclear robots to navigate complex radiation environments effectively. Pursuing these research avenues will advance nuclear robot technology and bolster their role in ensuring human safety in the nuclear energy sector.

2. Experimental Sample and Preparation

2.1. Experimental Sample

The key systems of nuclear robots include the sensing system, drive system, energy system, and control system. A working logic diagram of a remote-control robot is illustrated in Figure 1, drawn using Photoshop.

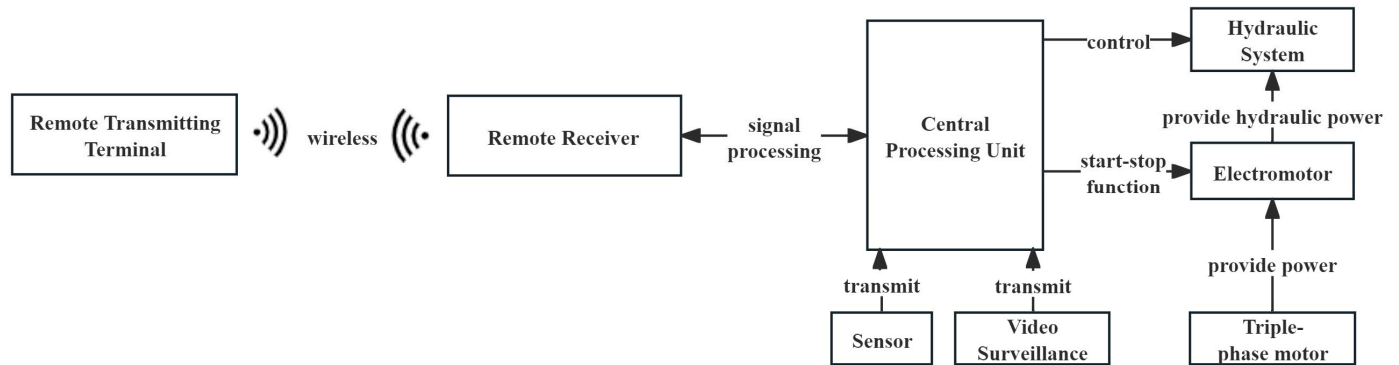


Figure 1. Working logic diagram of remote-control robot.

In the experimental research of this paper, the control system mainly includes relays, transformers, circuit breakers, phase-sequence protection relays, thermal overload relays, a DC contactor, and controllers. The sensing system mainly includes Hall sensors, pressure transducers, and temperature transducers. Simultaneously, experiments were conducted on five sets of devices, and the control group was established to reduce the impact of individual differences on the experimental results. The list of irradiation experiment samples in the structure of the robot’s control and sensing systems is shown in Table 1. During the experiments, the samples were placed as sets in the irradiation chamber. Five sets of device samples and four sets of lithium battery samples were labeled, and the operational status and key parameters were meticulously recorded at different irradiation total doses.

Table 1. Experimental model.

No.	Device	Model	Quantity	Manufacturer	Key Parameter
1	Hall sensors	DW-AS-624-M8-001	5	Contrinex	Contrinex inductive proximity sensor, tubular, 8 mm diameter × 35 mm body, 304 stainless steel housing, PNP, N.C. output, 2 mm sensing distance, flush, 5 kHz switching frequency, IP67, 3-pin M8 quick-disconnect.
2	Pressure transducers	MIK-P300	5	MEACON	Provides measurement accuracy up to 0.05%FS. The pressure range is 0~150 Mpa, 180 Mpa, 200 Mpa, 220 Mpa
3	Temperature transducers	MIK-WZPK-G	5	MEACON	a mineral insulated resistance thermometers, a wide range of temperatures, from −200 °C to +500 °C, Tolerance (°C) ± (0.15 + 0.002 t)
4	Relays	JD2912-1Z-24VCD	5	WUASO	Nominal Current Rating: 40 A/60 A, working Voltage:12 V/24 V, working temperature: −25 °C~+100 °C
5	Transformers	QUINT-PS/3AC/24DC/20	5	PHOENIX CONTACT	Primary-switched power supply unit QUINT POWER, Screw connection, SFB Technology (Selective Fuse Breaking), input: 3-phase, output: 24 V DC/20 A

Table 1. Cont.

No.	Device	Model	Quantity	Manufacturer	Key Parameter
6	Circuit breakers	NXB-63a	5	CHNT	Switch Type: ON + OFF, Latching Mechanical life: 20,000 times Tripping mode: Over-current tripping device Number of Pole: 2P Rated Voltage: 6000 (V) Material: Plastic, Electric Components
7	Phase-sequence relays	NJB1-X1	5	CHNT	Rated operational voltage: 200 V~500 V Operation time: phase sequence, phase failure ≤ 0.1 s 3.3 Contact capacity: Ue/Ie: AC-15 220 V/0.75 A, 380V/0.47 A; Ith: 3 A Mounting type: rail type, installation type Power consumption: ≤ 3 VA Note: In normal operation, the NO contact of the relay is closed, the operation indicator is on.
8	Thermal overload relays	JR36-20	5	CHNT	Altitude: no more than 2000 m; Ambient temperature: -50 °C~ $+40$ °C Relative humidity: no more than 50% when the highest temperature is $+40$ °C Rated insulation voltage (Ui) 380 V RConventional heating current (Ith) 5 A
9	DC contactor	NC1-0910Z	5	CHNT	3 NO Main Poles + 1 NO Auxiliary, 24 V DC Coil AC1:20A AC3:9A KW:4
10	Controllers	CR0232	5	Mobilsteuerung	Operating voltage [V]10...32 DC Total number of inputs and outputs: 80 a variety of input and output interfaces and functions
11	Battery	Ternary lithium /Lithium iron phosphate	4	CHNT	Ternary lithium: 12 V/2200 mAh 3.7 V/1300 mAh /Lithium iron phosphate: 12.8 V/800 mAh 3.2 V/1500 mAh

2.2. Experimental Conditions

In the experiment, ^{60}Co provided by the China Institute of Atomic Energy (CIAE) was used as the experimental source of γ -ray ionizing radiation. The γ -ray energy was 1.17 MeV and 1.33 MeV, the average activity of the radioactive source was 90 kCi, and the radiation field non-uniformity was less than 10%. The ambient temperature was 20 °C. The total radiation dose was measured using a silver dichromate chemical dosimeter, and the dose rate was calculated as the ratio of the total ionizing dose to the irradiation time. The silver dichromate chemical dosimeter is located above the controller and sensor. To ensure the consistency of the control box, one is placed at each of the four corners of the control box. All experimental samples were placed around a cylindrical radioactive source. The uncertainty in the dose rate measurements was less than 5%. The experiment monitored samples irradiated under 180 to 800 Gy/h. Figure 2 shows a similar experiment site, with each sample placed around a cylindrical radiation source. Figure 3 shows the schematic diagram of the position of the experimental sample.

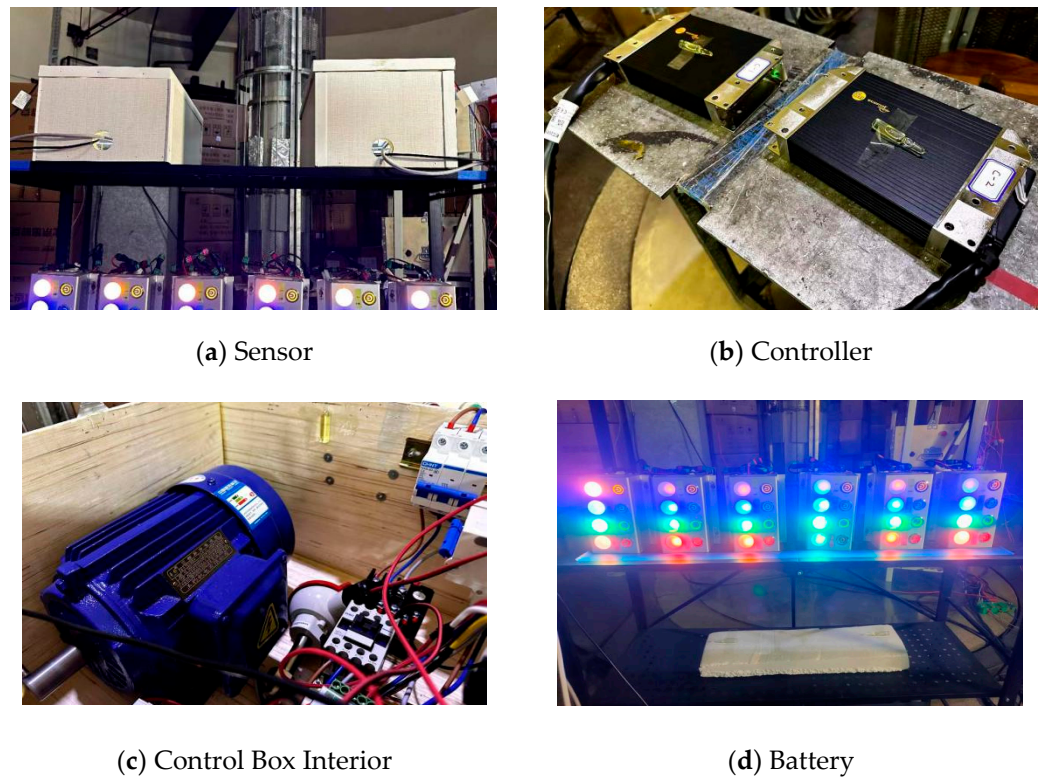


Figure 2. Experimental site.

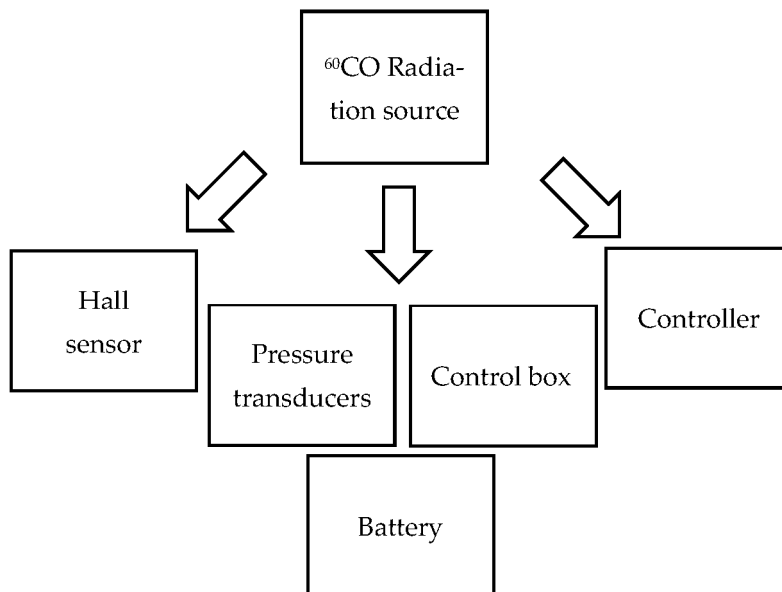


Figure 3. Experimental sample location diagram.

2.3. Experimental Detection Method

In Table 2, the definition criteria for the failure of each sensor and control system device are established. When the abnormal runout of the Hall sensor voltage value is greater than 5 V for two consecutive measurements, the abnormal runout of the pressure transmitter pressure value is abnormal twice for two consecutive measurements, or the abnormal runout of the controller voltage value and the temperature transmitter temperature value is greater than 10 V for two consecutive measurements, the device is considered to be invalid. Other control system components, such as transformers, DC contactors, circuit breakers, phase-sequence relays, and thermal overload relays, are deemed to have failed the first

time a function is lost or the indicator light is turned off. In the experiment, the pressure transmitter was tested at a dose rate of 180 Gy/h, the lithium battery was tested at a dose rate of 500 Gy/h, and the other devices were tested at a dose rate of 800 Gy/h, reaching a cumulative irradiation time of 4.5 h.

Table 2. Experimental detection method.

Device	Dose Rate	Time	Parameter	Failure State
Hall sensors	From 180 Gy/h to 800 Gy/h	4.5 h	Voltage (V)	Greater than 5 V for two consecutive measurements
Pressure transducers			Pressure (KPa)	Doubled twice consecutively
Temperature transducers			Temperature (°C)	Greater than 10 V for two consecutive measurements
Transformers			Output voltage (V)	The function is missing or the indicator is off for the first time
DC contactor			Coil voltage (V)	The function is missing or the indicator is off for the first time
Circuit breakers			Circuit connectivity	The function is missing or the indicator is off for the first time
Phase-sequence relays			Circuit connectivity	The function is missing or the indicator is off for the first time
Thermal overload relays			Circuit connectivity	The function is missing or the indicator is off for the first time
Controllers			Feedback signal	Feedback signal error /signal interruption
Relays			Output voltage (V)	Greater than 10 V for two consecutive measurements
Battery			Output voltage (V)	Greater than 5 V for two consecutive measurements

3. Experimental Results and Discussion

3.1. Sensing System Radiation Damage

In Table 3, the experimental results show Group A’s Hall sensor experienced damage and failure at 90 min, while the remaining four groups exhibited voltage fluctuations during the 4.5-h experiment without damage. It can be concluded that Hall sensors exhibit a tendency for stochastic radiation damage when the total dose exceeds 1200 Gy, among which only Group A experienced damage in the 4.5 h experiment.

Table 3. Cumulative failure dose (Gy) and First Failure Time (min) of different components of the sensor system.

Device \ Group	First Failure Time (min)	A	B	C	D	E
Hall sensors	90	1200	\	\	\	\
Pressure transducers	60	830	897	\	\	1030
Temperature transducers	100	2400	2267	3133	1333	1466

For the pressure transducers, radiation experiments were first performed on Groups A, B, and E devices at a dose of 180Gy/h within the first 210 min, and then the radiation dose was adjusted to 800 Gy/h. Pressure transducers of Groups A, B, and E experienced damage at 225, 230, and 240 min, respectively. If the pressure transducers are placed at 800 Gy/h, the first failure time is 60 min. When the total radiation dose exceeded 900 Gy, the pressure transducers began to exhibit deterministic damage effects. In the course of the

4.5-h experiment, all three devices were not spared damage, and the probability of damage reached 100%.

For the temperature transducers, during the test, the temperature measurement across the entire indoor environment will exhibit fluctuations. Therefore, if the measured value fluctuates by more than 10 degrees Celsius in either direction, it is considered indicative of equipment damage. A, B, C, D, and E experienced malfunctions at 180 min, 170 min, 235 min, 100 min, and 110 min, respectively. It can be inferred that deterministic radiation damage occurs when the total dose reaches 1333 Gy. The fault probability of each device increases gradually, and the fault probability reaches 100%.

Despite their susceptibility to radiation damage at higher doses, these sensors could still be valuable for routine maintenance and inspection tasks in nuclear facilities. They could assist in identifying abnormalities or potential issues in equipment or infrastructure, allowing for timely intervention and maintenance. Moreover, they could be used in controlled laboratory settings or low-radiation environments to conduct experiments, gather data, and improve sensor technologies for future applications in high-radiation environments.

The Hall sensor used in this experiment is a metal inductive sensor. Gamma rays induce ionization effects in materials, generating numerous free electrons and positive ions. These electrons and positive ions can influence the operation of the sensor through electromagnetic induction. In an inductive sensor, the free electrons generated by gamma rays may cause changes in the electric field distribution inside the sensor, thereby causing variations in the electrical parameters of components such as conductors or transformers, and even leading to transient faults or permanent damage to the sensor.

The pressure transducers typically incorporate a piezoresistive sensor, which is susceptible to failure akin to a silicon-integrated circuit. Radiation exposure can induce alterations in the lattice structure of the oxide layer material and affect the carrier density within it, consequently influencing conductance [13,18–20]. Correlations may exist between changes in conductance and radiation dosage, yielding predictable variations at particular radiation levels. While the illustrated temperature sensor employs a type K thermocouple, the electronic components driving it may succumb to radiation-induced failure.

3.2. Control System Radiation Damage

The experimental results in Table 4 indicate that in the control system, the relay, circuit breaker, continuous protection relay, overheat relay, and DC contactor have been tested under the radiation condition of 800 Gy/h for 4.5 h, operating stably with no abnormal phenomena and maintaining normal function. The probability of damage for these devices is zero if the cumulative radiation dose does not exceed 3600 Gy.

Table 4. Cumulative failure Dose (Gy) of different components of the control system.

Device	Group	A	B	C	D	E
Relays		\	\	\	\	\
Transformers		173	293	173	200	173
Circuit breakers		\	\	\	\	\
Phase-sequence relays		\	\	\	\	\
Thermal overload relays		\	\	\	\	\
Dc contactor		\	\	\	\	\
Controllers		116	125	116	144	129

Compared to other devices, transformers exhibit significantly lower radiation resistance performance. Failures occurred in transformers A, B, C, D, and E at 15, 22, 13, 13, and 14 min, respectively. It can be concluded that transformers demonstrate a deterministic radiation damage effect, with the damage probability reaching 100% when the total dose reaches 293 Gy.

Experimental data results show that the radiation resistance performance of the controller is similar to that of the transformer. When the accumulated radiation dose reaches

144 or above for the five groups of samples, all devices are damaged. The time of damage for the five groups of devices is similar, exhibiting deterministic radiation damage effects. After the experiment, the controller was sent back to the factory for maintenance, and internal components including the processor, power module, and communication module were replaced, but the controller still failed to work properly. Radiation not only damages the mainboard of the controller but may also affect the processor, power module, and communication module. Compared to other components of the system, the internal complex electronic components of transformers and controllers, such as integrated circuits, CMOS transistors, etc., are more susceptible to the effects of total radiation dose. The threshold voltage of electronic components is affected by radiation effects, leading to the loss or fluctuation of pulse signals in transformers and controllers [21]. This type of radiation damage may exhibit a deterministic trend within a certain range of radiation doses, leading to damage after reaching a certain radiation dose.

3.3. Battery Radiation Damage

In Figure 4, drawn using Origin, test-1 and test-2 are the experimental results of discharge voltage before irradiation, and Rad is the experimental results of discharge voltage TEST during irradiation. The results indicate that compared to the non-irradiated lithium iron phosphate batteries, the discharge voltage trend of a single 3.2 V lithium iron phosphate battery is largely unaffected by ionizing radiation. However, for the 12 V lithium iron phosphate battery pack, the rate of decrease in discharge voltage accelerates after irradiation, with a sharp drop during discharge at 270 min from 12.5 V to 7.4 V. Regarding ternary lithium batteries, individual cells of 3.7 V demonstrate better radiation resistance, but for the 12 V battery pack, the magnitude of the discharge voltage drop over the same period after irradiation is greater than before irradiation. This may be because the negative electrode of the battery is made of graphene material. While individual battery graphene sizes are small, battery pack sizes are large, resulting in a larger irradiation area. As the size increases, more electron-hole pairs are generated, leading to more oxide trap charges, resulting in significant degradation of carrier mobility [22,23]. Such changes can lead to a decrease in electrolyte conductivity and an increase in internal resistance, and consequently affect battery performance.

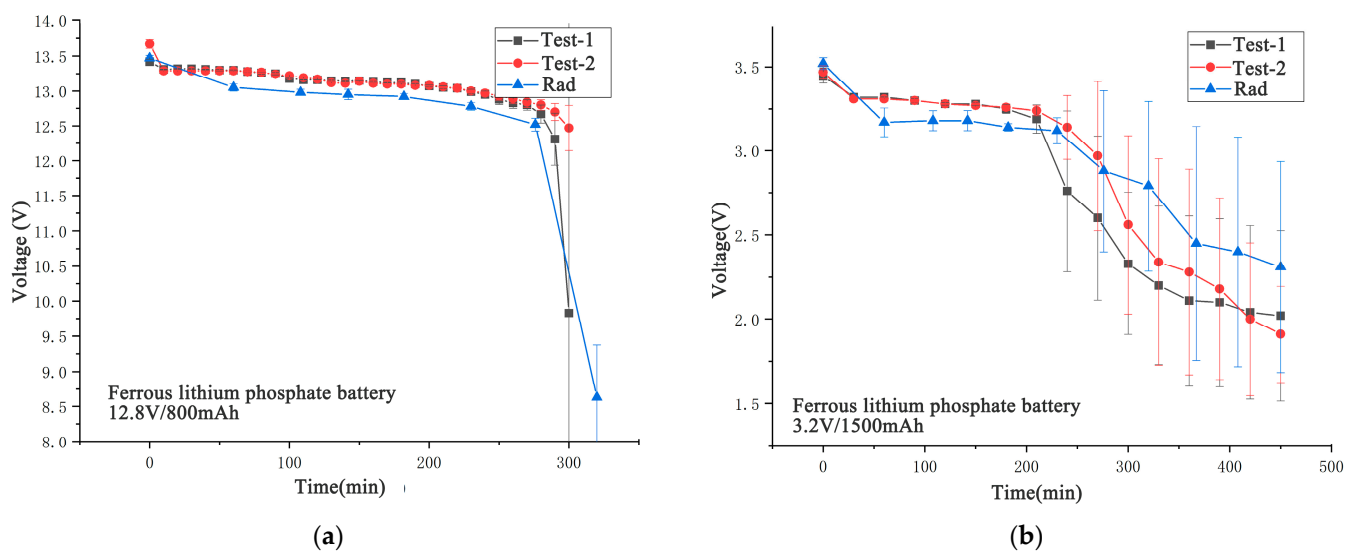


Figure 4. Cont.

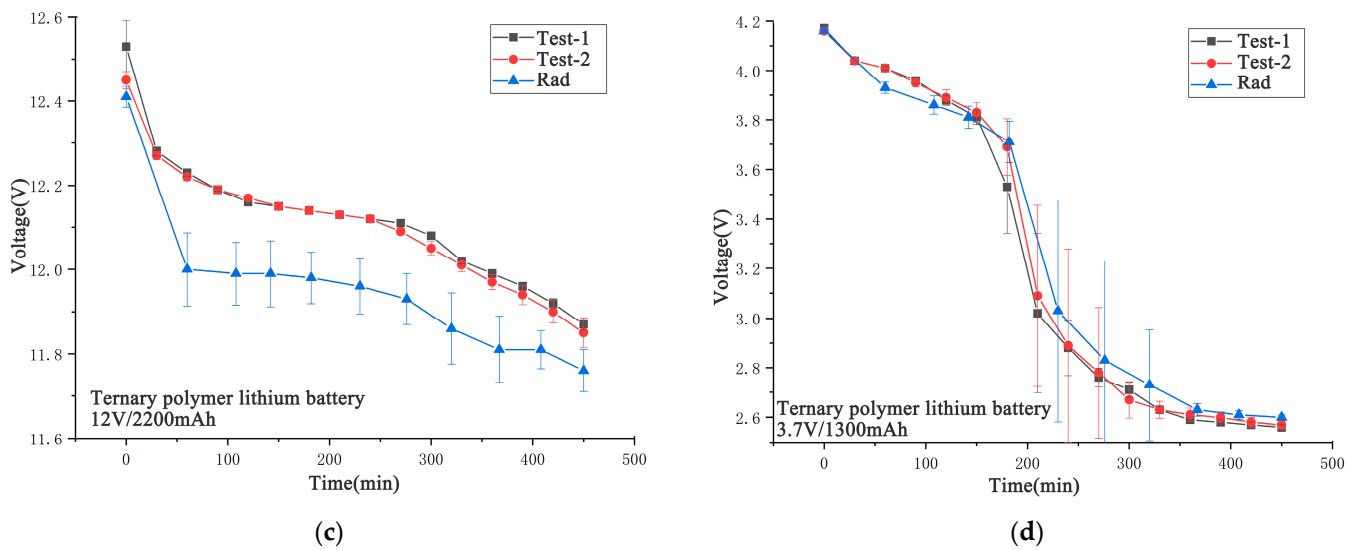


Figure 4. Radiation effect on lithium battery voltage diagram. (a) 12.8 V lithium iron phosphate battery voltage change; (b) 3.2 V lithium iron phosphate battery voltage change; (c) 12V ternary lithium battery voltage changes; (d) 3.7V ternary lithium battery voltage changes.

4. Shielding Reinforcement of Control and Sensing System Research

4.1. Radiation-Resistant Shielding Reinforcement Structure Design

According to the above experimental results, various types have good radiation resistance performance with a radiation endurance of over 800 Gy. The small size of the sensors facilitates replacement, essentially meeting the operational requirements of nuclear robots. However, transformers and controllers in the control system have a damage threshold range of only 110 Gy to 300 Gy, and their large size makes replacement inconvenient. The malfunction caused by radiation damage to transformers and controllers will render the robot unable to operate properly. As current industrial-grade controllers and transformers lack universal radiation-resistant models and such equipment requires extremely high radiation resistance, the most effective method is to use shielding structures for radiation protection. Figure 5 illustrates the design of the shielding structure for the robot control box. Considering the large number of control system components, the experiment contemplates placing all control system components in the same control box to provide radiation shielding reinforcement for the entire control box. In designing the shielding box structure, several factors must be considered: ① determining the dimensions of each component in the control box; ② reasonably arranging the layout of various components of the control system within the control box; and ③ determining the overall size of the shielding enclosure. Pb or W is typically chosen as the shielding material for large shielding structures.

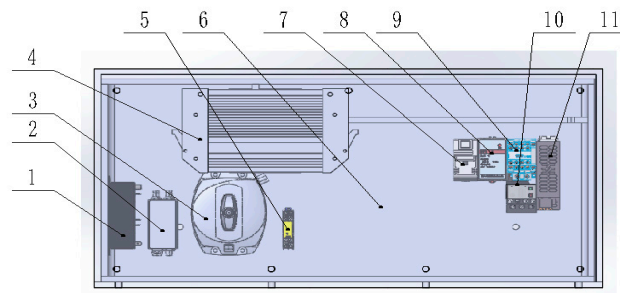


Figure 5. Shielding structure design of control Box 1. Emergency battery 2. Fiber optic media converter 3. Signal receiver 4. Master controller 5. Repeater 6. Electric control box shielding structure 7. Circuit breaker 8. Phase sequence protection relay 9. Dc contactor 10. Thermal overload relay 11. transformer.

4.2. Simulation Shielding Calculation and Analysis

The following data were collected in Super MC. This paper utilizes Super MC [24] (the neutron transport design and safety evaluation software system developed by the Phoenix Team at the Institute of Nuclear Safety Technology, Chinese Academy of Sciences) particle transport computational simulation software to design anti-radiation hardening shielding technology. Figure 6, drawn using Origin, illustrated the dose distribution in the control box. The cumulative dose is significantly higher on the side of the control box closer to the radioactive source compared to the other side. The sensitive components such as transformers, signal receivers, etc., are positioned in the middle to minimize exposure to radiation from the edges. Pb and W are used as shielding materials against ionizing radiation, and the control system is placed behind the robot in combination with factors such as the design margin and allowable weight gain, so as to optimize the robot's weight distribution and maintain overall balance.

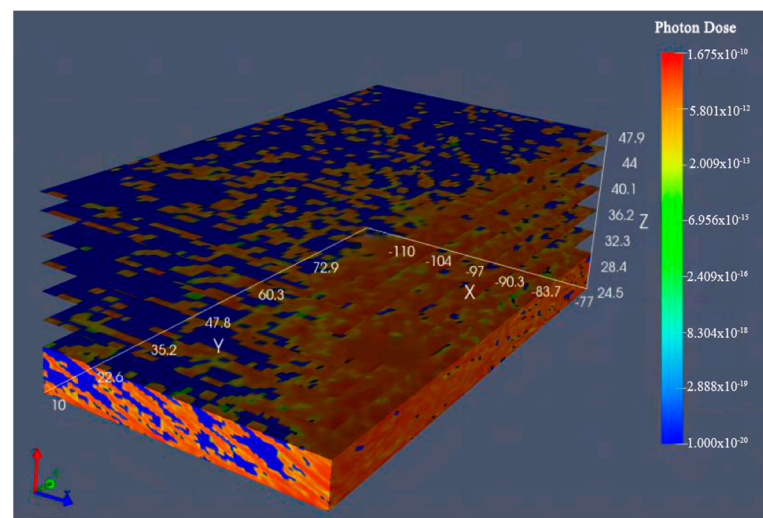


Figure 6. Control box dose distribution diagram.

Using Pb and W as shielding materials in simulation calculations, we compared the cumulative dose of each device under Pb and W shielding materials. Figure 7, drawn using Origin, displays the relationship between the cumulative dose of electrical components inside the control box and the shielding thickness. The simulation results indicate that as the thickness of the shielding layer increases, the cumulative dose received by all components decreases significantly. From the experimental results shown above, it can be seen that the controller and transformer have the worst radiation resistance performance among the control system devices, so the shielding effect on the controller and transformer should be considered when performing shielding reinforcement.

Figure 7 illustrates the shielding effects of Pb and W materials with varying thicknesses. As the shielding layer thickness increases, there is a notable decrease in the cumulative dose experienced by the controller under both Pb and W shielding materials. Specifically, with a 5 mm shielding layer thickness, the shielding rate of the controller increases by approximately 53.02% under Pb and 67.88% under W shielding. This rate further increases to approximately 74.89% under Pb and 86.17% under W when the thickness is increased to 10 mm. At 15 mm thickness, Pb achieves a shielding rate of 84.99% and W reaches 92.23%, while at a 20 mm thickness, Pb and W achieve shielding rates of 89.55% and 95.34%, respectively. Comparative results show that at a 5 mm shielding layer thickness, W has a significant advantage over Pb in shielding rate, with a difference of approximately 14.86%. The shielding rate of W is higher than Pb under all shielding thicknesses. Lead, with its dense composition and high atomic number, excels at effectively blocking high-energy rays like gamma rays. Conversely, tungsten, boasting even greater density and a higher atomic number, exhibits potentially superior shielding efficiency against higher-energy

rays. This distinction arises from their unique physical properties and atomic structures, influencing their interaction with various types of radiation. Although W still performs better, Pb's shielding rate improves faster, and the shielding rate of the two is gradually approaching. This provides some data support for the radiation resistance reinforcement of robots, and especially when considering material selection and shielding layer thickness, various factors need to be comprehensively considered.

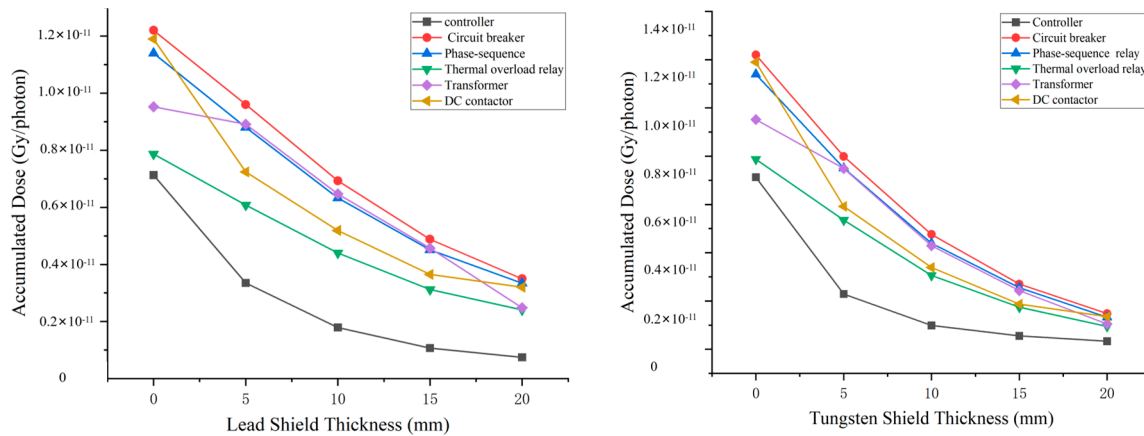


Figure 7. Schematic diagram of cumulative dose results for the control system.

Similarly, when the shielding layer thickness is 5 mm, the shielding rate of the transformer is approximately 6.41% under Pb shielding and 21.32% under W shielding. This rate increases to approximately 32.04% under Pb and 54.94% under W when the thickness is increased to 10 mm. At 15 mm thickness, Pb achieves a shielding rate of approximately 52.00%, while W reaches 74.47%. Finally, at 20 mm thickness, Pb and W achieve shielding rates of 66.39% and 88.97%, respectively.

The continuous increase in the shielding rate indicates that augmenting the thickness of the shielding layer effectively enhances the shielding rate, particularly for W. When the shielding layer thickness reaches 15 mm, the marginal contribution to the shielding rate is the most significant. These findings offer valuable data support for reinforcing robots against radiation, especially in practical applications where selecting appropriate shielding layer thickness and material combinations is crucial for achieving optimal shielding rates. Moreover, positioning the control box of nuclear robots at the rear of the robot is essential. The design of the control box structure not only effectively addresses the robot's counterweight issues but also ensures its balance and stability during operation. Through thoughtful design and layout, the shielding structure aims to mitigate potential uneven load distribution that robots may encounter during movement, thereby enhancing overall performance and operational reliability.

5. Conclusions

This paper conducts in-depth research on the principles of radiation shielding and the effects of radiation damage, carries out ionizing radiation experiments, establishes three-dimensional model simulations, and reinforces the shielding structure of vulnerable areas to enhance the stability of robots in ionizing radiation environments. The results show that Hall sensors, pressure transducers, temperature transducers, transformers, and controllers are damaged after reaching an accumulated radiation dose of 110 Gy. Lithium batteries have a minor impact on radiation mechanisms with increasing radiation doses, while relays, circuit breakers, phase sequence protection relays, overload relays, and DC contactors in the control system do not experience damage when the total dose does not exceed 3600 Gy. Simulation using Super MC yields the shielding performance of Pb and W against gamma rays at different thicknesses. Increasing the thickness of the shielding layer has a positive effect on both Pb and W. When the thickness of the shielding layer is 15 mm,

the marginal benefit of the shielding rate is the best. The shielding rate of the controller and transformer increased by approximately 84.99% and 52.00%, respectively, under Pb shielding, while that of W is 92.23% and 74.47%. Additionally, the control box is normally located at the rear of the robot. In order to enhance the operational capability of the robot in radiation environments without compromising its structural reliability, a radiation-resistant reinforcement structure is employed for the controller, serving as a counterweight for the robot. However, under certain circumstances, the shielding performance may fall short of ideal. Therefore, it is essential to comprehensively consider other factors based on different situations, such as minimizing proximity to radiation sources, replacing devices' radiation-resistant materials, or utilizing chips with inherent radiation-resistant properties. Therefore, the research findings of this paper validate the radiation resistance performance of various components within the control and sensing systems, offering vital data and theoretical backing for reinforcing the radiation resilience of nuclear robots.

Author Contributions: Conceptualization, Y.C. and S.X.; data curation, G.L. and C.W.; formal analysis, Y.C. and C.W.; funding acquisition, S.X.; investigation, S.Z.; methodology, D.T.; software, D.T. and S.Z.; supervision, S.X.; writing—original draft, Y.C. and S.X.; writing—review and editing, Y.C. All authors have read and agreed to the published version of the manuscript.

Funding: This research is funded by the National Natural Science Foundation of China (11905102).

Data Availability Statement: The data presented in this study are available upon request from the corresponding author.

Acknowledgments: The authors would like to express their sincere gratitude to the China Institute of Atomic Energy for providing the ^{60}Co γ source and the nuclear radiation detector.

Conflicts of Interest: The authors declare no conflicts of interest.

References

1. Liu, Q.; Zhang, Y.; Xiang, Y.; Huang, W.; Qian, J.; Dong, Y. The current situation and development trend of robot technology in nuclear power plants. *J. Robot. Appl.* **2011**, *24*, 12–16.
2. Liu, C.; Yan, Z.; Deng, J.; Zhang, B.; Guo, L. Research status and key technology analysis of emergency robots in nuclear power plants. *Nucl. Sci. Eng.* **2013**, *33*, 97–105. [CrossRef]
3. Han, Y.; Chi, X.; Wang, C.; Wang, C.; Liang, R.; Li, G.; Chen, F.; Sheng, Y.; Sun, Y. Application design of radiation-resistant robots in nuclear facility decommissioning scenarios. *Nucl. Electron. Detect. Technol.* **2022**, *406*, 992–999.
4. Liu, Z. Evaluation of radiation resistance performance of satellite power system based on QUM. Master's Thesis, National University of Defense Technology, Changsha, China, 2016. Available online: https://kns.cnki.net/kcms2/article/abstract?v=gr2ERH1EIEsFCB7Gj0SSrPsP2zOxpSoXU21Bm-r5vEptwGKm8RMleztTWiwXSzfDZBvqswuaDiNs0K0eVheIIIS15IiHcggWlbTvMrpRvoYe2FdyHNU7Dp8z7IeDmK_B3n6JvJ4eKPTIQuALkd6stA==&uniplatform=NZKPT&language=CHS (accessed on 13 February 2024).
5. Chen, F.; Zhu, W.; Dong, Q.; Han, Y.; Yan, S.; Shen, H. Radiation-resistant design and testing of remote-controlled robots. *Nucl. Electron. Detect. Technol.* **2016**, *36*, 121–124. Available online: <https://kns.cnki.net/kcms2/article/abstract?v=gr2ERH1EIEttbrw0ifDaKqAtby-VWi5NtA6ooAeBRaG6cSfXM8E2ELPT-G997G14xqsvZZt6h4HS04OQwSMhnN9xNzz9u-lF2HXl3zzlspUIYh2XzXAckQUok-Z2v3-R5PFul4QsswjeeHD3xFEhbA==&uniplatform=NZKPT&language=CHS> (accessed on 13 February 2024).
6. Su, K.; Yang, F.; Chen, Y. Design of special robot joint module and radiation protection. *Nucl. Electron. Detect. Technol.* **2023**, *6*, 56–61. [CrossRef]
7. Laurent, P.H. Robotics and Radiation Hardening in Nuclear. Industry 2000. Ph.D. Thesis, University of Florida, Gainesville, FL, USA, 2000.
8. Tang, B.; Wang, Z.; Liu, M.; Xiao, Z.; Zhang, Y.; Huang, S. Simulation test research on ionizing radiation damage of charge-coupled devices. *J. Electron.* **2010**, *38*, 1192–1195.
9. Li, J. Electron and Proton Radiation and Comprehensive Radiation Damage of Amorphous SiO₂ Thin Film for MOS Devices. Master's Thesis, Harbin Institute of Technology, Harbin, China, 2022.
10. Zhao, M. Study on Radiation Damage of Silicon-Based Power VDMOS Devices. Ph.D. Thesis, Harbin Institute of Technology, Harbin, China, 2021.
11. Li, L. Research on Displacement Damage Mechanism and Reinforcement Key Technology of MOS-Controlled Thyristor. Ph.D. Thesis, University of Electronic Science and Technology of China, Chengdu, China, 2021.
12. Jiang, M. Damage Effects of Single-Crystal Silicon Solar Cells under Proton, Electron, and Comprehensive Irradiation. Ph.D. Thesis, Harbin Institute of Technology, Harbin, China, 2015.

13. Jiang, H. Study on Radiation Damage Effects of HfO₂-Based MIS Capacitors. Ph.D. Thesis, Harbin Institute of Technology, Harbin, China, 2022.
14. He, B.; Wang, G.; Zhou, H.; Luo, Y.; Jiang, J. Comparison of radiation damage in NMOSFET devices with different sources and different γ dose rates. *J. Electron.* **2002**, 1229–1231. Available online: https://kns.cnki.net/kcms2/article/abstract?v=gr2ERH1EIEtB1u5RpQpk8mIEuWdDTML4SD9XMDZQMy9UY5_uga-2Bfk7RV_J2tj9YgLiFnw5sNkYptYMQzOAPh5-2bpLVQicUXK3ZocBt7n9MA3mHw-l-6nQ_WScrJjUoyVwYz_k3A=&uniplatform=NZKPT&language=CHS (accessed on 13 February 2024).
15. Ren, D.; Yu, X.; Ai, E.; Zhang, G.; Lu, F.; Guo, Q.; Fan, L.; Yan, R. Hot carrier damage of MOS capacitors and its relationship with ionizing radiation damage. *Prog. Solid-State Electron.* **2001**, 103–108. Available online: https://kns.cnki.net/kcms2/article/abstract?v=gr2ERH1EIEvSSfztAC_EOLw7VOMNSPqPKIaOj3jERfDDGnO7qcacvWgfQqop-M21Dyi32JDKQ6QBwRzLvRTFXDloEhK9tCxz6P25zTWTIa-mNdHkvxnxBS_MLeWK4UHInW8Iz0s8Oj0=&uniplatform=NZKPT&language=CHS (accessed on 13 February 2024).
16. He, Z.; Chen, W.; Han, J.; Liu, X.; Li, N.; Chen, R.; Luo, Y.; Yao, Z.; Li, P.; Wu, D. Radiation Effects and Radiation Hardening Techniques of Novel Microsystems. *Sci. China Phys. Mech. Astron.* **2024**, 54, 5–22.
17. Xie, R.; Ge, C.; Zhou, X.; Zhou, X.; Cao, L.; Chen, L.; Wu, J.; Qiao, M. Total Dose Radiation Effects on Radiation Hardened LDMOS Devices. *Mod. Appl. Phys.* **2023**, 14, 172–177.
18. Lee, M.; Cho, S.; Lee, N.; Kim, J. Design for High Reliability of CMOS IC With Tolerance on Total Ionizing Dose Effect. *IEEE Trans. Nucl. Sci.* **2020**, 20, 459–467. [[CrossRef](#)]
19. Messenger, G.C.; Ash, M.S. *The Effects of Radiation of Electronic Systems*; Van Nostrand Reinhold Company: New York, NY, USA, 1986; pp. 1–20.
20. Chen, P. *Radiation Effects on Semiconductor Devices and Integrated Circuits*; National Defense Industry Press: Beijing, China, 2005; pp. 8–23.
21. Daniel, M. Fleetwood, Total-Ionizing-Dose Effects, Border Traps, and 1/f Noise in Emerging MOS Technologies. *IEEE Trans. Nucl. Sci.* **2020**, 67, 1216–1240.
22. Sato, S.; Beernink, K.; Ohshima, T. Degradation behavior of flexible a-Si/a-SiGe/a-SiGe triple-junction solar cells irradiated with protons. *IEEE J. Photovolt.* **2013**, 3, 1415–1422. [[CrossRef](#)]
23. Jun, I.; Xapsos, M.A.; Messenger, S.R.; Burke, E.A.; Walters, R.J.; Summers, G.P.; Jordan, T. Proton nonionizing energy loss (NIEL) for device applications. *IEEE Trans. Nucl. Sci.* **2003**, 50, 1924–1928.
24. Wu, Y. Multifunctional Neutronics Calculation Methodology and Program for Nuclear Design and Radiation Safety Evaluation. *Fusion Sci. Technol.* **2018**, 74, 321–329. [[CrossRef](#)]

Disclaimer/Publisher’s Note: The statements, opinions and data contained in all publications are solely those of the individual author(s) and contributor(s) and not of MDPI and/or the editor(s). MDPI and/or the editor(s) disclaim responsibility for any injury to people or property resulting from any ideas, methods, instructions or products referred to in the content.